

# Scaling properties of the critical behavior in the dilute antiferromagnet $\text{Fe}_{0.93}\text{Zn}_{0.07}\text{F}_2$

Z. Slanić and D. P. Belanger

*Department of Physics, University of California, Santa Cruz, CA 95064 USA*

J. A. Fernandez-Baca

*Solid State Division, Oak Ridge National Laboratory, Oak Ridge, TN 37831-6393 USA*

(October 30, 2018)

Critical scattering analyses for dilute antiferromagnets are made difficult by the lack of predicted theoretical line shapes beyond mean-field models. Nevertheless, with the use of some general scaling assumptions we have developed a procedure by which we can analyze the equilibrium critical scattering in these systems for  $H = 0$ , the random-exchange Ising model, and, more importantly, for  $H > 0$ , the random-field Ising model. Our new fitting approach, as opposed to the more conventional techniques, allows us to obtain the universal critical behavior exponents and amplitude ratios as well as the critical line shapes. We discuss the technique as applied to  $\text{Fe}_{0.93}\text{Zn}_{0.07}\text{F}_2$ . The general technique, however, should be applicable to other problems where the scattering line shapes are not well understood but scaling is expected to hold.

## I. INTRODUCTION

Characterizations of the critical behavior of model systems through experiments and simulations are essential to verify the validity of theoretical models of phase transitions. Scattering techniques are invaluable for characterizing the staggered magnetization (the order parameter),  $M_s$ , the antiferromagnetic fluctuation correlation length,  $\xi$ , and staggered susceptibility,  $\chi_s$ , as a function of temperature in pure and dilute antiferromagnets, which prove to be ideal physical realizations of many model systems. Neutron scattering has been particularly instrumental in studies of antiferromagnets<sup>1</sup>, though magnetic x-ray scattering has also been employed to a limited extent<sup>2</sup>. Likewise, pulsed heat and optical techniques<sup>3</sup> have been essential in determining the critical behavior of the specific heat,  $C_m$ . The Ising model is the simplest of systems, with each spin having only two possible states, and becomes an exact model for the anisotropic antiferromagnets as the temperature  $T$  approaches the transition temperature  $T_c$ . Three of the most fundamental phase transitions are the pure Ising model, the random-exchange Ising model (REIM) and the random-field Ising model (RFIM). The pure Ising model has the exact Onsager<sup>4</sup> solution for dimension  $d = 2$ . For  $d = 3$  only approximate renormalization solutions, simulations and expansions exist. Antiferromagnets exist with strong anisotropy, such as  $\text{FeF}_2$  for  $d = 3$ . This system exhibits universal Ising static critical behavior close to the transition temperature<sup>5-7</sup>. The random-exchange model system is realized when the magnetic ions are randomly substituted by diamagnetic ions in  $\text{Fe}_x\text{Zn}_{1-x}\text{F}_2$  for  $x > x_p$ , where  $x_p = 0.246$  is the percolation threshold for this body-centered tetragonal magnetic lattice if only the dominant next-nearest neighbor interaction<sup>8</sup> is considered. Below  $x_p$  no phase transition can occur for geometric connectivity reasons. The anisotropy increases as  $x$  decreases<sup>9</sup>. As a result of the high anisotropy for these systems measured using neutron scattering<sup>10</sup>, asymptotic Ising critical behavior is well followed in the reduced temperature range  $|t| = |(T - T_c)/T_c| < 10^{-2}$ , where  $T_c$  is the transition temperature<sup>6</sup>.

Various experimental techniques can be used to extract universal Ising parameters associated with the asymptotic critical behaviors in antiferromagnets<sup>11</sup>. The universal parameters accessible through scattering techniques include the exponents and amplitude ratios associated with the asymptotic power law behaviors

$$\xi = \xi_\sigma^\pm |t|^{-\nu} \quad , \quad (1)$$

where  $+$  and  $-$  refer to  $t > 0$  and  $t < 0$ , respectively,

$$M_s = M_o |t|^\beta \quad , \quad (2)$$

where  $M_o$  is nonzero for  $t < 0$  only,

$$\chi_s = \chi_\sigma^\pm |t|^{-\gamma} \quad , \quad (3)$$

and, for antiferromagnets with quenched randomness, the disconnected susceptibility

$$\chi_s^{dis} = \chi_o^{dis\pm} |t|^{-\bar{\gamma}} \quad (4)$$

for  $q \neq 0$ . Pulsed heat and optical techniques can be used to obtain the specific heat critical behavior,

$$C = A^\pm |t|^{-\alpha} + B \quad , \quad (5)$$

which becomes symmetric and logarithmic,

$$C = A \ln |t| \quad , \quad (6)$$

when  $\alpha \rightarrow 0$ .

Equations 1-6 represent the asymptotic behaviors exhibited for data with sufficiently small  $|t|$ . The range of asymptotic Ising behavior in anisotropic short-range interaction antiferromagnets, for example, is partly determined by the anisotropy strength. For example, whereas  $FeF_2$  shows<sup>5</sup> asymptotic behavior for  $|t| < 10^{-2}$ , the less anisotropic isomorph  $MnF_2$ <sup>12,13</sup> shows asymptotic behavior only for  $|t| < 10^{-3}$ . If data are taken outside the asymptotic range of  $|t|$ , but still within the critical region, fits to the power law expressions yield only effective exponents<sup>14</sup> and effective amplitude ratios. In such cases, it may be more effective to use scaling function analyses, which include crossover to asymptotic critical behaviors, when some quantity such as the applied field,  $H$ , can be varied. We will briefly discuss this with regard to specific heat analyses done principally using  $Fe_{0.93}Zn_{0.07}F_2$  data. Scaling functions are also of great utility in fitting scattering data when the line shapes are not well known. For example, at constant  $H$  in the asymptotic region, we can use the fact that the scaling functions can depend only on  $|q|/\kappa$ , where  $q$  is the distance from the antiferromagnetic Bragg scattering point, (100) for  $FeF_2$ , in reciprocal lattice units (rlu) and  $\kappa = 1/\xi$  is the reciprocal correlation length for antiferromagnetic fluctuations. In this work, we will show how the general properties of the scaling functions can be utilized to advantage in the characterization of the random-exchange and random-field scattering data obtained<sup>15</sup> using  $Fe_{0.93}Zn_{0.07}F_2$ . However, the technique has more general utility; it can be used in any case where theory does not provide adequate models of scattering functions but scaling is expected to hold.

## II. SPECIFIC HEAT SCALING

Although we primarily focus here on the scaling behavior of the critical scattering of the  $d = 3$  dilute antiferromagnet, it is instructive to review briefly the success of scaling analyses in the study of the specific heat critical behavior in the same system. Not only will this demonstrate the usefulness of the scaling approach, it will highlight the results for the specific heat behavior, which are complementary to the scattering results but show the largest discrepancy with simulation results for the RFIM. This will be important in our later assessment of the agreement between simulations and experimental results.

In zero field, the dilute anisotropic antiferromagnet is predicted to have a transition described by the random-exchange Ising model. One of the most striking changes in the critical behavior induced by random quenched dilution is observed in the specific heat for  $d = 3$ . Whereas the pure  $FeF_2$  sample shows  $\alpha = 0.11$ , in agreement with theory<sup>16</sup>, the Harris criterion imposes the constraint that  $\alpha < 0$  upon dilution. Indeed, the exponent has been found<sup>17</sup> to be  $\alpha = -0.10 \pm 0.02$  experimentally. Monte Carlo studies also yield a negative value<sup>18</sup>. Interestingly, with the application of a field, the RFIM specific heat is again found to be divergent in experiments<sup>17</sup>, with  $\alpha \approx 0$ , as discussed below.

One way to utilize scaling functions is to attempt to collapse the experimental data onto a scaling function of the appropriate scaling argument. The collapse will only work well if the critical parameters used in the data collapse are correct. The RFIM scaling behavior of the free energy, for example, is expected to have the form<sup>11</sup>

$$F \sim H^{2(2-\alpha)/\phi_{RF}} g(|t_H| H^{-2/\phi_{RF}}) \quad , \quad (7)$$

where  $t_H = (T - T_N + bH^2)/T_N$ ,  $T_N$  is the zero-field transition temperature,  $b$  is a small mean-field (MF) parameter,  $\alpha$  is the zero-field specific heat exponent, and  $\phi_{RF}$  is the RFIM crossover exponent. When a new phase transition occurs at  $T = T_c(H)$ , the asymptotic limit of the specific heat can be obtained<sup>19</sup> from the free energy in the limit  $|t| \rightarrow 0$

$$C = \frac{\partial^2 F}{\partial T^2} = H^{-2\alpha/\phi_{RF}} g'(|t_H| H^{-2/\phi_{RF}}) \sim H^{2(\bar{\alpha}-\alpha)/\phi_{RF}} |t|^{-\bar{\alpha}} \quad , \quad (8)$$

where  $t = (T - T_c(H))/T_c(H)$ . For  $\bar{\alpha} = 0$ , this becomes

$$C \sim H^{-2\alpha/\phi_{RF}} \ln |t| \quad , \quad (9)$$

which is symmetric above and below  $T_c(H)$ . Note that the field dependence of the peak amplitude is dependent on  $\bar{\alpha}$ . In the scaling plots, both the shape and the field dependent amplitude must be correct for the data to collapse onto a single scaling function.

The scaling behavior of the specific heat has been experimentally demonstrated for both  $d = 2$ , where no transition takes place<sup>20</sup>, and  $d = 3$ , where a new transition occurs<sup>17</sup>. In both cases, the critical parameters can be determined accurately by the quality of the data collapse onto a single scaling function. The most accurate measurements have been obtained using the optical linear birefringence technique which has been shown to faithfully represent the magnetic specific heat behavior<sup>3,17,21</sup>. It was shown that the experimental data for the  $d = 3$  system  $Fe_{0.93}Zn_{0.07}F_2$ , when divided by  $H^{-2\alpha/\phi_{RF}}$ , collapse onto a single scaling function if  $\alpha = -0.10 \pm 0.02$  and  $\phi_{RF} = 1.42 \pm 0.03$ , the latter having been determined by measurements on  $Fe_xZn_{1-x}F_2$  with several different concentrations<sup>22</sup> and predicted<sup>23</sup> to be a few percent larger than the zero-field staggered susceptibility exponent measured<sup>24</sup> to be  $\gamma = 1.31 \pm 0.03$ . Note that if the RFIM specific heat exponent  $\bar{\alpha} = 0$ , as indicated by the asymptotic shape of the curve, the random-exchange exponent must have the value  $\alpha = -0.10 \pm 0.02$ , which is consistent with the earlier value  $\alpha = -0.09 \pm 0.03$  obtained<sup>25</sup> by fitting the data from a lower magnetic concentration sample with  $x = 0.60$  to a power law. Hence, both the shape and field-dependent amplitude of the critical peak are consistent with  $\bar{\alpha} = 0$ , i.e. a symmetric, logarithmic divergence.

Further evidence that  $\bar{\alpha}$  is close to zero is obtained from Faraday rotation experiments under constant field or constant temperature. Faraday measurements yield the critical behavior of the specific heat, but with a different field amplitude than the specific heat peaks. Near the phase transition it was shown by Kleemann, et al.<sup>19</sup>, that

$$\frac{\partial M}{\partial T} = \frac{\partial^2 F}{\partial H \partial T} \sim H^{2(1+\bar{\alpha}-\alpha-\phi_{RF}/2)/\phi_{RF}} |t|^{-\bar{\alpha}} \quad , \quad (10)$$

which becomes, for  $\bar{\alpha} = 0$ ,

$$\frac{\partial M}{\partial T} \sim H^{2(1-\alpha-\phi_{RF}/2)/\phi_{RF}} \ln |t| \quad , \quad (11)$$

and

$$\frac{\partial M}{\partial H} = \frac{\partial^2 F}{\partial H^2} \sim H^{2(2+\bar{\alpha}-\alpha-\phi_{RF})/\phi_{RF}} |t|^{-\bar{\alpha}} \quad , \quad (12)$$

which becomes, for  $\bar{\alpha} = 0$ ,

$$\frac{\partial M}{\partial H} \sim H^{2(2-\alpha-\phi_{RF})/\phi_{RF}} \ln |t| \quad . \quad (13)$$

The field dependent amplitudes of logarithmic peaks have been measured with the results  $2(1 - \alpha - \phi_{RF}/2)/\phi_{RF} \approx 0.56$  and  $2(2 - \alpha - \phi_{RF})/\phi_{RF} \approx 0.97$ . With the measured value  $\phi_{RF} = 1.42 \pm 0.03$ , these two equations yield  $\alpha = -0.11 \pm 0.02$  and  $\alpha = -0.11 \pm 0.04$ , respectively. These values are consistent with the values  $\alpha = -0.10 \pm 0.02$  from the  $Fe_{0.93}Zn_{0.07}F_2$  experiment<sup>17</sup> and  $\alpha = -0.09 \pm 0.03$  from the  $Fe_{0.60}Zn_{0.40}F_2$  experiment<sup>25</sup>. Hence, the field dependent amplitudes as well as the peak shapes are all consistent with  $\bar{\alpha} \approx 0$ . A scaling analysis would similarly require  $\bar{\alpha} \approx 0$  in the case of Faraday rotation for a good data collapse. The result  $\bar{\alpha} \approx 0$  from experiments contradicts the Monte Carlo result<sup>26</sup>  $\bar{\alpha} = -0.5 \pm 0.2$ .

### III. SCATTERING SCALING FUNCTION

We next turn to the scattering function, which should obey scaling properties close to  $T_c(H)$ . Within the static approximation<sup>1</sup>, the intensity of the magnetic critical scattering from high quality single crystal magnetic systems is proportional to the Fourier transform of the spin-spin correlation function  $S(q) = [\langle s_q s_{-q} \rangle]$  convoluted with the instrumental resolution, where the  $\langle \rangle$  brackets signify a thermal average and the  $[ ]$  brackets signify a configurational average.

The spin-spin correlation can be expressed as

$$S(q) = \chi_s + \chi_s^{dis} \quad , \quad (14)$$

where

$$\chi_s = [\langle s_q s_{-q} \rangle - \langle s_q \rangle \langle s_{-q} \rangle] \quad (15)$$

is the staggered susceptibility and

$$\chi_s^{dis} = [\langle s_q \rangle \langle s_{-q} \rangle] \quad (16)$$

is the disconnected susceptibility. For line shapes obtained at one value of the field, we expect a scaling function that only depends on the ratio  $|q|/\kappa$  of the two physically relevant inverse length scales. For  $|q| > 0$ ,

$$\chi_s(q) = A^\pm \kappa^{\eta-2} f(q/\kappa) \quad . \quad (17)$$

For pure, translationally invariant systems  $\chi_s^{dis} = M_s^2 \delta(q)$ . For random systems, on the other hand,  $\chi_s^{dis}$  may have a  $q$  dependent contribution. In particular, in RFIM systems, such a term is induced by the random field, giving<sup>11</sup> for  $|q| > 0$  at constant  $H$ ,

$$\chi_s^{dis}(q) = A^\pm B^\pm \kappa^{\bar{\eta}-4} g(q/\kappa) \quad . \quad (18)$$

Hence,  $S(q)$  involves two possibly independent scaling functions,  $f(q/\kappa)$  and  $g(q/\kappa)$  and two possibly independent exponents  $\eta$  and  $\bar{\eta}$ . This makes the method of collapsing data onto scaling functions extremely difficult since the contributions to the data from the two scaling functions are not easily separable.

To fit the data we must, in principle, use data only in the range of small  $\kappa$  (i.e. small  $|t|$ ) and  $|q|$  in order to be sure we are dealing with asymptotic behavior. In the study of  $FeF_2$ , data were used in the range  $|t| < 10^{-2}$  to obtain the most reliable exponents and amplitude ratios, since this was shown to be in the asymptotic range for pure Ising behavior in specific heat critical behavior<sup>5</sup> measurements. In the  $Fe_{0.93}Zn_{0.07}F_2$  experiments, we used data for  $|t| < 10^{-2}$  since this is the range for which the specific heat shows the RFIM logarithmic behavior<sup>17</sup>. However, we typically use a wide range of  $|q|$ . The crossover at large  $|q|$  is relatively unimportant since the critical scattering intensity becomes very small. On the other hand, including data at large  $|q|$  helps to set the level of background scattering.

Many scattering critical behavior analyses are done using the simple MF Lorentzian for  $|q| > 0$ ,

$$f(q) = \frac{A^\pm}{1 + q^2/\kappa^2} \quad , \quad (19)$$

giving

$$S(q) = \chi_s(q) = \frac{A^\pm}{q^2 + \kappa^2} \quad (20)$$

for  $q \neq 0$ , consistent with the fact that  $\eta = 0$  in MF. Since the upper critical dimension,  $d_u$ , above which the MF equations are correct, is four or greater, the Lorentzian line shape can only be approximate for three dimensions. Deviations from the MF Lorentzian line shape should become evident as one approaches the transition temperature and are generally found to be much more important below the transition temperature. This has been discussed with respect to the pure  $d = 3$  Ising antiferromagnet  $FeF_2$ <sup>6</sup>. Scattering data for  $FeF_2$  were analyzed using approximations to the line shapes by Fisher and Burford<sup>27</sup> (BF) for  $T > T_N$ ,

$$f(q/\kappa) \propto \frac{(1 + \phi^2 q^2/\kappa^2)^{\eta/2}}{1 + \psi q^2/\kappa^2} \quad , \quad (21)$$

and by Tarko and Fisher<sup>28</sup> (TF) for  $T < T_N$ ,

$$f(q/\kappa) \propto \frac{(1 + \phi'^2 q^2/\kappa^2)^{\sigma+\eta/2}}{(1 + \psi' q^2/\kappa^2)(1 + \phi''^2 q^2/\kappa^2)^\sigma} \quad , \quad (22)$$

where  $\phi$ ,  $\phi'$ ,  $\phi''$ ,  $\sigma$ ,  $\psi = 1 + 1/2\eta\phi^2$  and  $\psi' = 1 + 1/2\eta\phi'^2 + \sigma(\phi'^2 - \phi''^2)$  are fixed to values determined from the numerical studies. The values are given in Table I. The expressions have the correct scaling behavior in the limits  $|q|/\kappa \rightarrow 0$  and  $|q|/\kappa \rightarrow \infty$  and serve as appropriate interpolation functions between those limits. We show the critical exponents and amplitude ratios obtained from fits of the data obtained for  $10^{-4} < |t| < 10^{-2}$  using these scaling forms in Table I as well as theoretically determined universal critical parameters. The experimental and theoretical values serve to contrast those from similar analyses done on the diluted system  $Fe_{0.93}Zn_{0.07}F_2$  to be discussed next. The corrections to MF are only significant for  $|t| < 10^{-3}$  and are most significant for  $T < T_N$ . Since many  $d = 3$  studies do not probe critical behavior any closer than this to  $T_c$ , the Lorentzian line shape generally serves satisfactorily for

extracting estimates of the critical exponents. Obviously, more precise measurements that probe regions of smaller  $|t|$  can yield much more accurate critical parameters, but only if a suitable line shape is used.

Data for the pure  $d = 2$  case of  $K_2CoF_4$  has been analyzed in a similar manner<sup>29</sup>. In this case  $\eta = 0.25$  and an analysis using the MF Lorentzian fails markedly below  $T_N$ . The appropriate TF and FB equations, in contrast, yield critical behavior consistent with the  $d = 2$  Ising model.

The scattering function for the dilute antiferromagnet is predicted to have an additional term not present in the pure case<sup>30</sup> that may affect experimentally determined to corrections to scaling and, possibly, measurements of the amplitude ratio for  $\chi_s$ . The exponents are probably not influenced since this extra contribution vanishes as  $T \rightarrow T_N$ . A fit to a simple Lorentzian seems to work reasonably well for data with  $|t| < 10^{-3}$  in the very dilute antiferromagnet  $Fe_{0.46}Zn_{0.54}F_2$ . For the random-exchange Ising model<sup>16</sup>,  $\eta \approx 0.04$ , which is similar to the value for the pure case. Hence, it is reasonable that the Lorentzian line shape works well in this reduced temperature range just as it does in the pure  $d = 3$  Ising case. For data closer to  $T_c$ , however, just as in the pure case, we would expect deviations from the MF Lorentzian, particularly for  $T < T_c$ . Unlike the Tarko-Fisher case for the pure Ising model, no approximants have been worked out for the random-exchange model for use in data analyses beyond MF. One possible approach is to use the same TF and FB expressions developed for the pure case. This assumes that the line shapes for the pure and REIM are very similar. Such an approach was successfully employed to analyze the data for the dilute  $d = 2$  antiferromagnet<sup>31</sup>. Another strategy is to use the same forms, but to let the TF/FB parameters be free fitting parameters. Such functions would satisfy scaling in the proper limits and would hopefully be very good interpolative functions between those limits. We will describe below results for  $Fe_{0.93}Zn_{0.07}F_2$  obtained using the latter of these two methods.

We next turn to the more difficult case of the random-field scattering in  $Fe_{0.93}Zn_{0.07}F_2$ , which occurs for  $H > 0$ . In the case studied  $H = 7T$ . We expect the scattering function for  $|q| > 0$  to be

$$S(q) = A^\pm \kappa^{\eta-2} f(q/\kappa) + B^\pm A^{\pm 2} \kappa^{\bar{\eta}-4} g(q/\kappa) \quad . \quad (23)$$

Taking into consideration the instrumental resolution as well as the two separate scaling functions, there is little chance of using the data directly to determine the two independent scaling functions. Hence, we must start with model functions and test their appropriateness. The first natural test functions to use in the data analysis are the MF scaling ones<sup>32</sup>,

$$S(q) = \frac{A^\pm \kappa^{-2}}{1 + q^2/\kappa^2} + \frac{B^\pm \kappa^{-2}}{(1 + q^2/\kappa^2)^2} \quad , \quad (24)$$

where we might expect the amplitudes  $A^\pm$  and  $B^\pm$  to be temperature dependent, since  $\eta$  and  $\bar{\eta}$  are not, in fact, zero. We did such an analysis previously<sup>33</sup> and found reasonable fits at all temperatures in the sense that the line shapes yielded values of  $\kappa$  and  $\chi_s = A^\pm \kappa^{-2}$ . However, when an attempt was made to fit these values to power law behaviors, reasonable results were obtained above the transition but not below. The results above  $T_c(H)$  are  $\nu = 0.90 \pm 0.01$  and  $\gamma = 1.72 \pm 0.02$ . These values are consistent with results above  $T_c(H)$ , obtained<sup>34</sup> for  $x = 0.6$  using a MF analysis. At these lower concentrations, equilibrium critical behavior is not obtained below  $T_c(H)$ , but the data analysis was done well above  $T_c(H)$  where equilibrium prevails.

We note that the failure of the MF analysis below  $T_c(H)$  is very similar to the situation observed<sup>29</sup> in the pure  $d = 2$  antiferromagnet  $K_2CoF_4$ . The MF equations fail in that case because  $d = 2$  is far from the upper critical dimension  $d_u = 4$  and  $\eta = 0.25$  in contrast with the pure  $d = 3$  case where  $\eta = 0.04$ . The TF expression developed for  $d = 2$  served nicely for the data analysis and agreement was found with theory. Interestingly, the FB scaling function for  $T > T_N$  is not very different from the MF one. For the  $d = 3$  RFIM, the value of  $\eta$  is predicted to be even larger, perhaps as large as  $\eta = 0.5$ . Hence, it is not that surprising that the MF data analysis fails below  $T_c(H)$  in this case. To proceed, we must go beyond a simple MF line shape analysis.

Since there is not yet a theoretical line shape available beyond MF, we must try to use scaling properties to guide us. However, if there are two independent scaling functions, as in Eq. 24, the task becomes formidable. Fortunately, there are two approximations motivated by theoretical<sup>35</sup> and simulation<sup>18</sup> works. The first is that  $\bar{\eta} = 2\eta$ , a limiting case of the Schwartz-Soffer<sup>36</sup> inequality  $\bar{\eta} \leq 2\eta$ . The second is that  $g(q/\kappa) = f^2(q/\kappa)$  is a very good approximation. We adopt these two simplifications, making the scattering function for  $|q| > 0$  the more manageable expression

$$S(q) = A^\pm \kappa^{\eta-2} f(q/\kappa)(1 + B^\pm A^{\pm 2} \kappa^{\eta-2} f(q/\kappa)) \quad . \quad (25)$$

It is not clear at this point how accurate these approximations are. However, it is not possible to proceed without them and they appear to be well justified. It is highly unlikely that experiments will be able to test the validity of the assumptions directly. Only further theoretical progress can provide a better starting point for the data analysis. Note that the MF expression in Eq. 24 is a special case of this for  $\eta = 0$ . We are still faced with the correction to

instrumental resolution, however, which itself depends on the line shape we are trying to determine<sup>6</sup>. Hence, it is still hard to scale the data directly without an explicit functional form for  $f(q/\kappa)$ . To simplify the procedure further, therefore, we have adopted as our scaling functions the TF and FB scaling functions except that we allow all the parameters to vary. Hence, we are assured of the proper scaling in the limiting cases of  $|q| \rightarrow 0$  and  $\kappa \rightarrow 0$  and hopefully the interpolation between these limits will be adequate with the parameters determined from the fits of the data. Unfortunately, the usual technique of fitting each scan separately, where a scan is made in  $q$  at fixed  $T$ , and then extracting the exponents from power law fits to the resulting  $\kappa$  and  $\chi_s$  cannot work well since there are now so many free parameters, including the various exponents, amplitudes and the TF/FB parameters. We can, however, fit all the data scans simultaneously, since the line shape parameters are all the same for every temperature for  $T < T_c$  and  $T > T_c$  and the critical exponents are the same for all  $T$ . The new technique has the advantage over the more classic technique in that the line shape does not need to be known beforehand. In the RFIM, the line shape is both unknown and far from the MF prediction, so the classic method using the MF line shapes failed to yield the critical behavior parameters. Our new procedure using the TF and FB line shapes with variable parameters and fitting all the data simultaneously, on the other hand, was successfully employed for the  $H > 0$  random-field Ising behaviors in  $Fe_{0.93}Zn_{0.07}F_2$  and yielded both the critical behavior parameters and the critical scattering line shapes. Both the classic and new techniques worked well for the  $H = 0$  case in which the line shapes are nearly mean-field and much simpler than the RFIM ones. This demonstrates the reliability of the new technique and we can apply it with some confidence to the RFIM, where the more classical technique fails to yield results.

#### IV. EXPERIMENTAL AND FITTING DETAILS

Adding to the difficulty of implementing scaling in the scattering line shape analysis is the necessity to account for significant instrumental resolution corrections. The instrumental resolution can be measured for a particular spectrometer configuration by measuring the width of the magnetic Bragg scattering peak at low temperatures. The Bragg scans in the transverse, longitudinal and vertical directions well below the transition temperature yield the response to scattering from the Bragg peak. Theoretically, the Bragg peak is a delta function and in practice is much more narrow than the instrumental resolution in good quality crystals. Since the scattering in these anisotropic crystals is well described within the static approximation, the scans in the three directions yield the widths along the three principal axes of the resolution ellipsoid. If we have a theoretical line shape, we can use the measured Bragg scattering scans to numerically integrate the line shape which can then be compared directly with the scattering data. Alternatively, other groups have used Gaussian (or with less accuracy triangular) approximations to the Bragg scans and then analytically integrated to obtain the resolution corrections. In this study we exclusively use the numerical integration technique. For resolution curves measured at uniform steps in  $q$ , we have for the intensity in transverse data scans,

$$I(q) \sim \frac{\sum S((q - q_0 - a)^2 + b^2 + c^2)T_a L_b V_c}{\sum T_a L_b V_c}, \quad (26)$$

where the sums are over  $a$ ,  $b$ , and  $c$  and  $q_0$  accounts for imperfect alignment in the transverse direction. For a well aligned crystal,  $q_0$  is usually much smaller than the resolution width in the transverse direction. Misalignments along the vertical and longitudinal directions are generally inconsequential for a well aligned crystal since the resolutions are much coarser in these directions than in the transverse one.  $T_a$ ,  $L_b$  and  $V_c$  are the approximately Gaussian Bragg line shapes measured at low  $T$  using evenly spaced steps in  $q$ . This is the technique explained<sup>6</sup> in detail in the context of the study of  $FeF_2$ . If a crystal has a small mosaic, this can also be approximately taken into account in the same manner.

To fit the resolution-convoluted line shape to the scattering data, we use a nonlinear least squares fitting routine to determine the parameters of the theoretical line shape and critical exponents. Note that with each iteration of the fitting program, the line shape must be reintegrated over the resolution ellipsoid since the amount of correction from the resolution convolution depends on the line shape and, hence, the fitted parameters. Since the resolution correction in neutron scattering experiments is substantial and line shape dependent, it is very difficult to determine the line shape directly from the data. Hence, in the absence of a theoretical model, we must choose a trial function that satisfies the correct scaling requirements and allows suitable flexibility in the fits of the data. Our strategy is to use the TF and FB line shapes described above.

For the experiments we used two samples of  $Fe_{0.93}Zn_{0.07}F_2$ . One is the same large sample used in specific heat experiments<sup>17</sup>. It is somewhat irregular in shape and has a mass of 1.35 g. The magnetic concentration gradient limited the range of data unaffected by rounding to  $|t| > 1.15 \times 10^{-3}$ . The second is a slice cut from the large sample with its faces perpendicular to the magnetic concentration gradient. It is approximately one tenth the mass of the

original sample. The smaller sample was used to obtain data closer to the transition with  $|t| > 1.14 \times 10^{-4}$ . The data from both samples were used simultaneously in the data fits with different instrumental resolution corrections appropriate to the two samples and the spectrometer configurations used to make measurements on them. Neutron scattering measurements were made at the Oak Ridge National Laboratory High Flux Isotope Reactor using a two-axis spectrometer configuration. We used the (0 0 2) reflection of pyrolytic graphite (PG) at an energy of 14.7 meV to monochromate the beam. We mainly employed two different collimation configurations. The lower resolution, primarily used for the large sample, is with 70 min of arc before the monochromator, 20 before the sample and 20 after the sample. Primarily for the thin sample, we made scans with 10 min of arc before and after the sample. Two PG filters were used to eliminate higher-order scattering. The carbon thermometry scale was calibrated to agree with recent specific heat results<sup>17</sup> for the  $H = 0$  transition. The field dependence of the thermometry was also calibrated. All scans used in this report, other than those used for obtaining the resolution ellipsoid, are transverse ones about the (1 0 0) antiferromagnetic Bragg point.

## V. FITTING RESULTS

We applied the techniques described above to the random-exchange behavior ( $H = 0$ ), where there is only one term in the scattering function for  $|q| > 0$ . We first did the fits using the MF line shapes imposed by setting  $\sigma = 1$  and  $\phi$ ,  $\phi'$  and  $\phi''$  equal to zero. The results for the fitted critical parameters are essentially identical to the results from the conventional method of fitting each scan to obtain the temperature dependent correlation and susceptibility and subsequently fitting them to extract the exponents and amplitude ratios. The results are shown in Table I. We include the expressions for the normalized  $\overline{\chi^2}$  in the table, which are most useful for relative comparisons between fits. The values are not close enough to unity to consider the fitting functions statistically perfect ones. Very small systematic errors from the resolution corrections and the approximations in the line shapes can easily account for values of  $\overline{\chi^2}$  being somewhat larger than unity. The goodness of the fits are better judged from the scaling plots discussed below. The agreement between the two methods of fitting the data gives us some confidence in fitting the field data, for which the line shape is unknown, using the technique in which all data are simultaneously fit. We proceed beyond MF by doing the fits with the TF and BF parameters as free parameters. The fitting results are again shown in Table II. The range of data was restricted to the reduced temperature range  $|t| < 0.15$  and includes 2198 data. The results for the critical exponents and amplitudes are not very different from the previous result and the line shape is not very different from the MF one. When examining individual scans, we observe no systematic deviations of the data from the fit at any temperature for which data were included in the fit. We show representative scans in Fig. 1, including data above and below  $T_c$ . No systematic deviations of the data from the fits are evident, indicating that the line shapes work well for the data within the range of  $|t|$  used in the fits. To demonstrate that the data are well described by the fitted scaling function, we subtract the scattering background from them, deconvolute them with the instrumental resolution, divide them by  $A^\pm \kappa^{\eta-2}$  and plot them versus  $|q|/\kappa$  in Fig. 2. The data from the two samples are plotted separately, but the solid curves are identical in the two cases. The scatter of the data for the small sample simply reflects the smaller size and the resulting lower count rate. However, some of the data from the small sample are taken much closer to  $T_c$ , since the rounding from the concentration gradient is less significant. The data close to  $T_c$  are very important in the fits. The consistent results obtained using MF and scaling line shapes in the analyses give us confidence that the scaling technique may work well even in cases where the line shapes are very far from being MF, as in the RFIM case we describe next.

For the RFIM case, the procedure is identical to the random-exchange one above, except that the scattering function involves the more complicated expression in Eq. 25. In one fit, we restricted the data range to  $|t| < 10^{-2}$ , with 2444 data, since this is the temperature range over which the asymptotic logarithmic specific heat behavior is observed<sup>17</sup>. In a second fit, we further restricted the temperature range to  $|t| < 3 \times 10^{-3}$ , with 1000 data, to test whether crossover effects were still significant. The fitting results are shown in Table III. The two fits are rather consistent, suggesting that the results are close to the asymptotic ones. In Fig. 3 we show data and the corresponding fits for a few scans to show that there are no significant systematic deviations. After determining the line shape parameters and critical exponents, we used a procedure similar to that described above to demonstrate that the data collapse onto scaling functions for  $T < T_c$  and  $T > T_c$ . We subtracted the scattering background, deconvoluted the data with the instrumental resolutions, divided by  $A^\pm \kappa^{\eta-2}(1 + B^\pm A^\pm \kappa^{\eta-2} f(q/\kappa))$  and, for clarity, plotted the results versus  $\kappa_o^\pm |q|/\kappa$  instead of simply  $|q|/\kappa$  so that the data for  $T > T_c(H)$  and  $T < T_c(H)$  do not overlap. The results of this procedure are shown in Fig. 4. The data from the large and small samples are shown separately.

We have obtained from the scaling analysis not only the critical parameters but adequate approximations to the line shape scaling functions for both the  $d = 3$  random-exchange and random-field Ising models. We already have the  $d = 2$  and  $d = 3$  pure line shapes from the TF and FB expressions. It is instructive to compare all of these to

the MF Lorentzian line shapes. The comparisons are shown in Fig. 5, where we have plotted scaling functions versus  $|q|/\kappa$ . The upper plot is for  $T > T_c$  and the lower one for  $T < T_c$ . The lowest curve in each case represents the simple Lorentzian line shape that is accurate in the MF limit. The pure  $d = 3$  Ising model line shapes show nearly MF behavior for  $T > T_c$ . For  $T < T_c$ , more significant deviations from MF are apparent. This is consistent with the experimental results obtained using  $FeF_2$ . The  $d = 3$  experimental random-exchange scaling functions indicate that there is not much difference between the pure and random-exchange line shapes for  $d = 3$ . In contrast, for the random-field case, the deviations from MF found in the experiments are very large for  $T < T_c(H)$  in comparison to the pure and random-exchange  $d = 3$  Ising models. Even in the case for  $T > T_c(H)$  the deviations are large relative to the other  $d = 3$  models. The very large deviations for  $T < T_c(H)$  are consistent with the failure of the MF Lorentzian line shape in producing values for  $\kappa$  and  $\chi_s$  that obey power law behavior. For the pure  $d = 2$  Ising model, shown as a reference for non-MF behavior, the results for  $T < T_c(H)$  are the largest of the examples shown, whereas the behavior for  $T > T_c$  is not far from MF. We see from this comparison of the scaling functions, particularly for  $T < T_c$ , that MF behavior is fairly well followed for the  $d = 3$  pure and random-exchange models, whereas for the random-field case, where the upper critical dimension has significantly increased to  $d_u = 6$ , the line shapes are very non-Lorentzian. Determining the line shape from the scattering data is difficult. We have achieved an approximate determination of the proper line shapes. Once theoretical results give a more firm foundation for the trial function for the scattering line shape, we will be able to give a more concrete comparison of the experiments to theory and simulations.

In Table IV we show the results of the critical exponents for the specific heat and neutron scattering RFIM experiments compared with simulation results. For the pure  $d = 3$  Ising model, the experimentally determined universal exponents and amplitude ratios agree very well with theoretical and simulation results. The experimental results from neutron scattering were obtained using the TF and FB line shapes. The specific heat was obtained using both pulsed heat and birefringence techniques and clearly can be considered to be exceedingly well characterized. For the REIM, we again have excellent agreement between experiment and Monte Carlo simulations. The specific heat is determined most precisely using the birefringence technique, but the results are consistent with the pulsed heat data. This case can also be considered well characterized.

The RFIM case shows mixed results when the experimental exponents are compared with those from simulations. The scattering results for  $\nu$  and  $\gamma$  are quite consistent with the simulation values. The exponent  $\beta$  has not been reliably measured yet and its comparison with simulation results is very important. The most glaring inconsistency is between the simulation and experimental values of  $\alpha$ , where the experiments indicate a symmetric, logarithmic divergence and the simulations indicate a non-divergent peak. This inconsistency deserves further study.

Although we have achieved fits to the data obtained in equilibrium scattering experiments using  $Fe_{0.93}Zn_{0.07}F_2$ , the asymptotic behavior is only observed very close to  $T_c(H)$  at  $H = 7$  T. Our results may be somewhat influenced by the effects of crossover to random-exchange behavior. We hope in the future to do these experiments at much higher fields to ensure that the results we have obtained in this study are close to the asymptotic ones. In addition, by using apparatus capable of reaching much higher fields, we can study the scaling behavior of the scattering line shapes as a function of  $|t|H^{-2/\phi_{RF}}$  in a similar way to our treatment of the specific heat.

This work has been supported by DOE Grant No. DE-FG03-87ER45324 and by the Oak Ridge National Laboratory, which is managed by UT-Battelle, LLC, for the U.S. Dept. of Energy under contract DE-AC05-00OR22725.

<sup>1</sup> M. F. Collins, "Magnetic Critical Scattering", Oxford University Press, 1989.

<sup>2</sup> A. I. Goldman, K. Mohanty, G. Shirane, P. M. Horn, R. L. Green, C. J. Peters, T. R. Thurston, and R. J. Birgeneau, Phys. Rev. B **36**, 5609 (1987).

<sup>3</sup> J. Ferre and G. A. Gehring, Rep. Prog. Phys. **47**, 513 (1984).

<sup>4</sup> L. Onsager, Phys. Rev. **65**, 117 (1944).

<sup>5</sup> D. P. Belanger, P. Nordblad, A. R. King, V. Jaccarino, L. Lundgren and O. Beckman, J. Magn. Magn. Mater. **31-34**, 1095 (1983).

<sup>6</sup> D. P. Belanger and H. Yoshizawa, Phys. Rev. B **35**, 4823 (1987).

<sup>7</sup> G. K. Wertheim and D. N. E. Buchanan, Phys. Rev. **161** 478, (1967).

<sup>8</sup> C. D. Lorenz and R. M. Ziff, J. Phys. A **31**, 8147 (1998).

<sup>9</sup> C. B. de Araujo, Phys. Rev. B **22**, 266 (1980).

<sup>10</sup> M. T. Hutchings, B. D. Rainford and H. J. Guggenheim, J. Phys. C **3**, 307 (1970).

<sup>11</sup> For reviews, see D. P. Belanger and A. P. Young, J. Mag. Mag. Mater. **100** (1991) 272; D. P. Belanger, "Spin Glasses and Random Fields", ed. A. P. Young, World Scientific, 1998, pp. 251; T. Nattermann, *ibid.*, pp. 277.



- <sup>12</sup> J. Barak, V. Jaccarino and S. M. Rezende, *J. Magn. Magn. Mater.* **9**, 323 (1978).
- <sup>13</sup> O. Nikotin, P. A. Lingard and O. W. Dietrich, *J. Phys. C* **2**, 1168 (1969).
- <sup>14</sup> A. Aharony and G. Ahlers, *Phys. Rev. Lett.* **44**, 782 (1980).
- <sup>15</sup> Z. Slanič, D. P. Belanger and J. A. Fernandez-Baca, *Phys. Rev. Lett.* **82**, 426 (1999).
- <sup>16</sup> M. Campostrini, A. Pelissetto, P. Rossi and E. Vicari, cond-mat/9905078 (1999).
- <sup>17</sup> Z. Slanič and D. P. Belanger, *J. Magn. Magn. Mater.* **186**, 65 (1998).
- <sup>18</sup> H. G. Ballesteros, L. A. Fernandez, V. Martin-Mayor, A. M. Sudupe, G. Parisi and J. J. Ruiz-Lorenzo, *Phys. Rev. B* **58**, 2740 (1998).
- <sup>19</sup> W. Kleemann, A. R. King and V. Jaccarino, *Phys. Rev. B* **34**, 479 (1986).
- <sup>20</sup> I. B. Ferreira, A. R. King, V. Jaccarino, J. L. Cardy and H. J. Guggenheim, *Phys. Rev. B* **28**, 5192 (1983).
- <sup>21</sup> K. E. Dow and D. P. Belanger, *Phys. Rev. B* **39**, 4418 (1989).
- <sup>22</sup> I. B. Ferreira, A. R. King, V. Jaccarino, *Phys. Rev. B* **43**, 10797 (1991); *J. Appl. Phys.* **69**, 5246 (1991).
- <sup>23</sup> A. Aharony, *Europhys. Lett.* **1**, 617 (1986).
- <sup>24</sup> D. P. Belanger, A. R. King and V. Jaccarino, *Phys. Rev. B* **34**, 452 (1986).
- <sup>25</sup> R. J. Birgeneau, R. A. Cowley, G. Shirane, H. Yoshizawa, D. P. Belanger, A. R. King and V. Jaccarino, *Phys. Rev. B* **27**, 6747 (1983).
- <sup>26</sup> H. Rieger, *Phys. Rev. B* **52**, 6649 (1995).
- <sup>27</sup> M. E. Fisher and R. J. Burford, *Phys. Rev.* **156**, 583 (1967).
- <sup>28</sup> H. B. Tarko and M. E. Fisher, *Phys. Rev. B* **11**, 1217 (1975).
- <sup>29</sup> R. A. Cowley, M. Hagen and D. P. Belanger, *J. Phys. C* **17**, 3763 (1984).
- <sup>30</sup> R. A. Pelcovits and A. Aharony, *Phys. Rev. B* **31**, 350 (1985).
- <sup>31</sup> M. Hagen, R. A. Cowley, R. M. Nicklow and H. I. Ikeda, *Phys. Rev. B* **36**, 401 (1987).
- <sup>32</sup> G. Grinstein, S.-k. Ma and G. Mazenko, *Phys. Rev. B* **15**, 258 (1977).
- <sup>33</sup> Z. Slanič, D. P. Belanger and J. A. Fernandez-Baca, *J. Magn. Magn. Mater.* **177-181**, 171 (1998).
- <sup>34</sup> D. P. Belanger, A. R. King and V. Jaccarino, *Phys. Rev. B* **31**, 4538 (1985).
- <sup>35</sup> M. Gofman, J. Adler, A. Aharony, A. B. Harris and M. Schwartz, *Phys. Rev. B* **53**, 6362 (1996).
- <sup>36</sup> M. Schwartz and A. Soffer, *Phys. Rev. B* **33**, 2059 (1986).
- <sup>37</sup> R. Guida and J. Zinn-Justin, *J. Phys. A* **31**, 8103 (1998).
- <sup>38</sup> N. Rosov, A. Kleinhammes, P. Lidbjork, C. Hohenemser and M. Eibschutz, *Phys. Rev. B* **37**, 3265 (1988).
- <sup>39</sup> U. Nowak, K. D. Usadel and J. Esser, *Physica A* **250**, 1 (1998).
- <sup>40</sup> The only measurement is using the dilation technique at lower concentration were the system is not in equilibrium by C. A. Ramos, A. R. King, V. Jaccarino and S. M. Rezende, *J. de Phys.* **49**, C8-1241 (1988).
- <sup>41</sup> R. Folk, Yu. Holovatch and T. Yavors'kii, *Phys. Rev. B* **61**, 15114 (2000).

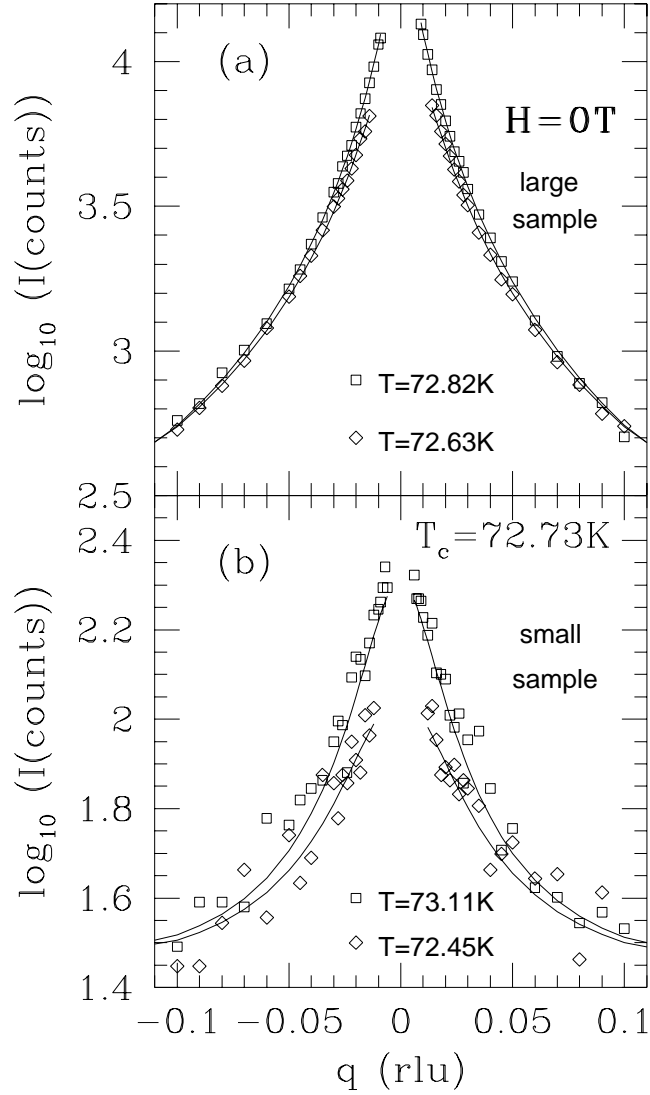


FIG. 1. The logarithm of the scattering intensity vs.  $q$  and the curves representing the corresponding fits for  $H = 0$ . One scan for  $T > T_c(H)$  and one for  $T < T_c(H)$  are shown for the large sample in figure a and similarly for the small sample in figure b.

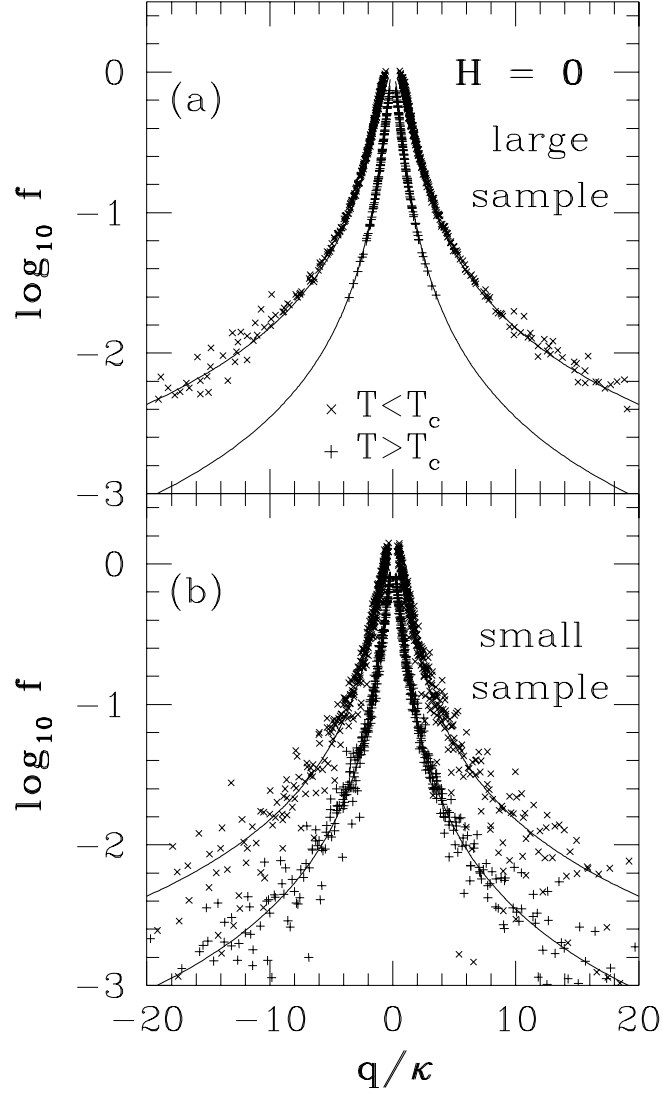


FIG. 2. Scaled neutron scattering data, deconvoluted with the instrumental resolution, taken at different temperatures at  $H = 0$  T collapsed onto the universal function  $f(q/\kappa)$ . The scatter in the small sample data is larger due to smaller number of counts obtained in the thin sample. The fit was made for  $|t| < 0.01$ . The solid curves, which are identical in the upper and lower plots, represent the line shapes for  $T > T_c$  and  $T < T_c$  determined from the fits to the data.

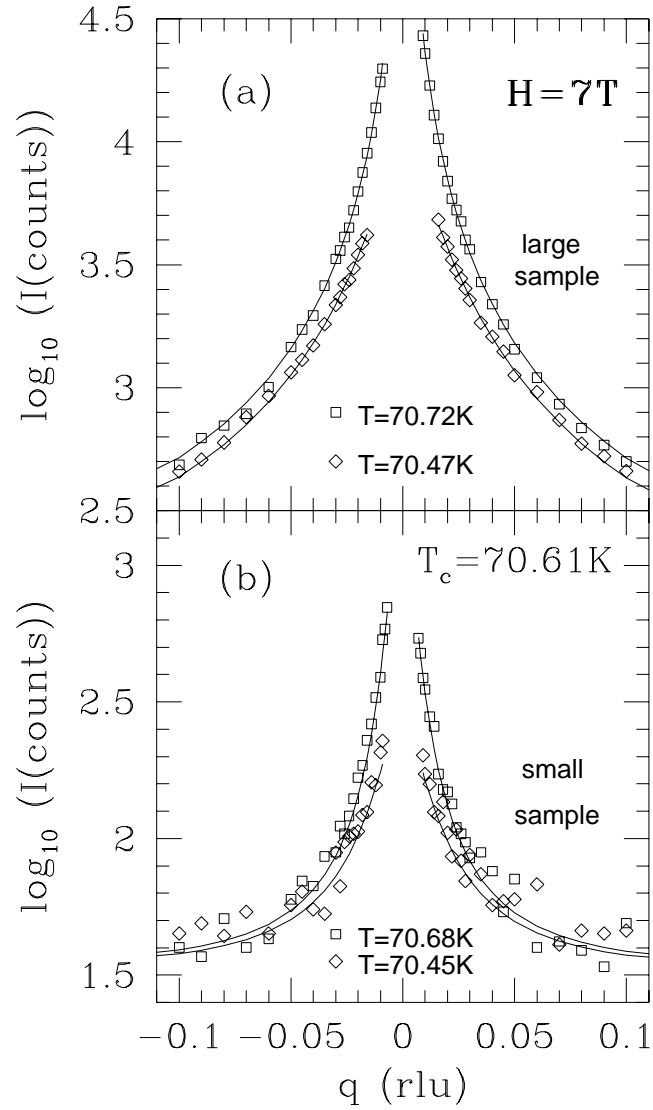


FIG. 3. The same as in Fig. 1, but for the the random-field Ising case  $H = 7\text{ T}$ .

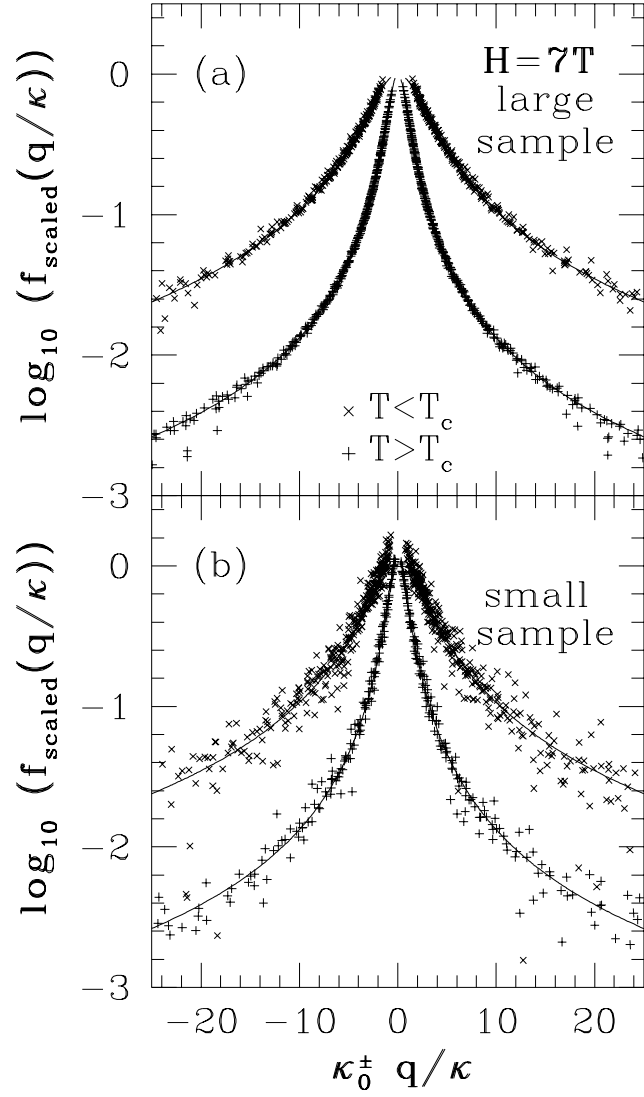


FIG. 4. The same as in Fig. 2, but for the random-field Ising case  $H = 7$  T. The fit was made for  $|t| < 0.01$ .

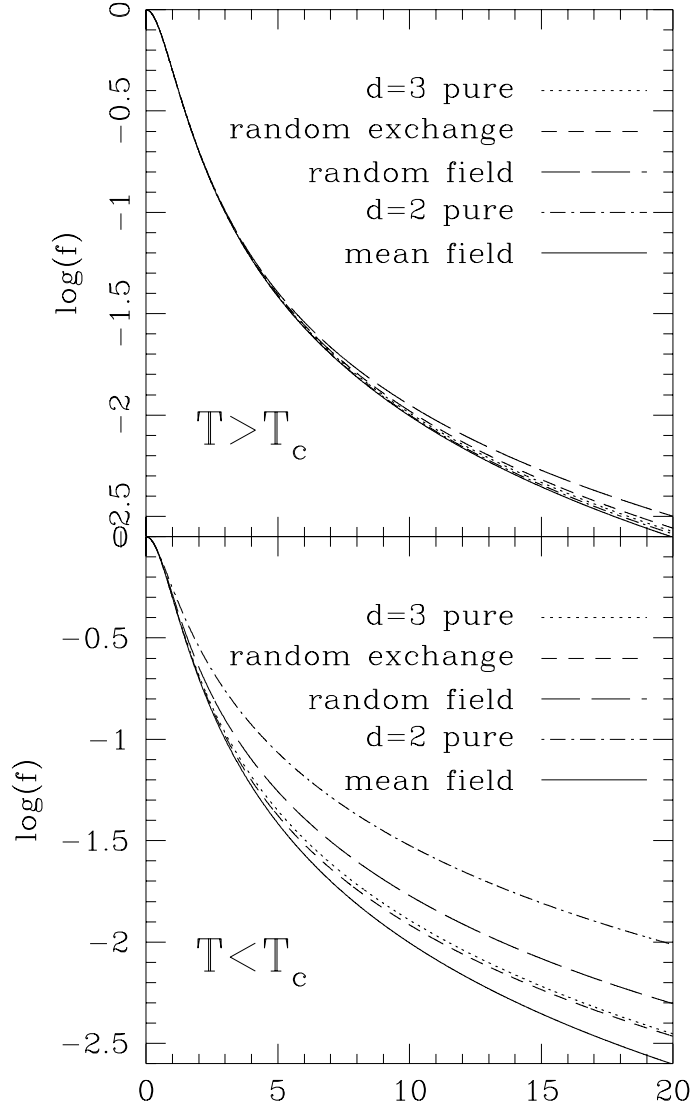


FIG. 5. A comparison of the logarithm of the scaling functions versus  $q/\kappa$  for different models. The pure cases are from the TF and FB expressions. The REIM and RFIM are from the experiments, as described in the text. Note that the corrections to the MF equation are largest below the transition. The random-field deviations for  $d = 3$  are greater than the pure and random-exchange, but are significantly smaller than the pure  $d = 2$  scaling function below the transition. Above the transition, all of the line shapes are close to MF.

parameter	FB and TF	$d = 3$ Ising <sup>16</sup>
$T_c$	$78.418 \pm 0.001$ K	
$\nu$	$0.64 \pm 0.01$	$0.63002 \pm 0.0023$
$\kappa_0^+/\kappa_0^-$	$0.53 \pm 0.01$	$0.510 \pm 0.002$
$\gamma$	$1.25 \pm 0.02$	$1.2371 \pm 0.004$
$\chi_0^+/\chi_0^-$	$4.6 \pm 0.2$	$4.77 \pm 0.02$
$\eta$	$0.056^*$	
$\psi$	$1.001^*$	
$\sigma$	$2\eta = 0.111^*$	
$\phi$	$0.15^*$	
$\phi'$	$0.3247^*$	
$\phi''$	$0.09355^*$	
$\psi'$	$1.0137^*$	

TABLE I. Experimental and Theoretical values for the critical parameters of the  $d = 3$  pure Ising model. Data were fit over the range  $10^{-4} < |t| < 10^{-2}$ . Note that  $\psi = 1 + 1/2\eta\phi^2$  and  $\psi' = 1 + 1/2\eta\phi'^2 + \sigma(\phi'^2 - \phi''^2)$ . Values marked with \* are fixed parameters in the fitting process.

parameter	Lorentzian	TF/FB
$T_c$ (fixed)	$72.73K^*$	$72.73K^*$
$\eta$	$0.079 \pm 0.010$	$0.079 \pm 0.012$
$\nu$	$0.70 \pm 0.03$	$0.70 \pm 0.02$
$A^+$	$7.66 \pm 0.15$	$7.59 \pm 0.10$
$A^-$	$6.71 \pm 0.10$	$6.42 \pm 0.10$
$\kappa_0^+$	$0.57 \pm 0.02$	$0.56 \pm 0.02$
$\kappa_0^-$	$1.21 \pm 0.10$	$1.13 \pm 0.05$
$\sigma$	$1^*$	$0.16 \pm 0.20$
$\phi$	$0^*$	$0.18 \pm 0.02$
$\phi'$	$0^*$	$0.18 \pm 0.02$
$\phi''$	$0^*$	$0.08 \pm 0.10$
$C$	$0.0142 \pm 0.0002$	$0.0142 \pm 0.0001$
$\chi^2$	2.0	1.7
No. pts.	2280	2198

TABLE II. The values found for the parameters from the fits for the  $H = 0$  T data. The exponents and amplitude ratios are defined in the text.  $C$  refers to a constant,  $q$ -independent background scattering term. The scattering data for the large sample were fit for  $|t| > 1.15 \times 10^{-3}$  and the data for the small sample were fit for  $|t| > 1.14 \times 10^{-4}$ .  $T_c$  was fixed in the case of the scattering fits. The first column of results is for the MF line shapes. The second is TF/FB using the pure line shape parameters. The third column is obtained by letting the TF/FB parameters be fit along with the exponents.

parameter	$ t  < 10^{-2}$	$ t  < 3 \times 10^{-3}$
$T_c$ (fixed)	70.61K*	70.61K*
$\eta$	$0.20 \pm 0.05$	$0.16 \pm 0.06$
$\nu$	$0.88 \pm 0.05$	$0.87 \pm 0.07$
$A^+$	$10.0 \pm 0.2$	$9.21 \pm 0.3$
$A^-$	$6.15 \pm 0.14$	$4.45 \pm 0.15$
$\kappa_0^+$	$1.13 \pm 0.04$	$0.95 \pm 0.17$
$\kappa_0^-$	$3.24 \pm 0.11$	$2.78 \pm 0.5$
$B^+$	$(4.7 \pm 0.1) \times 10^{-5}$	$(3.00 \pm 0.13) \times 10^{-5}$
$B^-$	$(4.0 \pm 0.3) \times 10^{-5}$	$(8.0 \pm 1.0) \times 10^{-5}$
$\sigma$	$0.67 \pm 0.5$	$0.86 \pm 0.6$
$\phi$	$0.16 \pm 0.04$	$0.08 \pm 0.01$
$\phi'$	$0.39 \pm 0.25$	$0.36 \pm 0.3$
$\phi''$	$0.31 \pm 0.25$	$0.26 \pm 0.2$
$C$	$0.017 \pm 0.001$	$0.016 \pm 0.001$
$\overline{\chi^2}$	3.07	2.3
No. pts.	2444	1000

TABLE III. The values found for the parameters from the TF/FB fits for the  $H = 7$  T data. The data for the large sample were fit for  $|t| > 1.15 \times 10^{-3}$  and the data for the small sample were fit for  $|t| > 1.14 \times 10^{-4}$ .  $T_c$  was fixed in the case of the scattering data.



Pure	$FeF_2$	Renormalization and High T Expansions
$\alpha$	$0.11 \pm 0.005^5$	$0.1099 \pm 0.0007^{16}$ $0.109 \pm 0.004^{37}$
$\beta$	$0.325 \pm 0.005^7$	$0.32648 \pm 0.00018^{16}$ $0.3258 \pm 0.0014^{37}$
$\nu$	$0.64 \pm 0.01^6$	$0.63002 \pm 0.00023^{16}$ $0.6304 \pm 0.0013^{37}$
$\gamma$	$1.25 \pm 0.02^6$	$1.2371 \pm 0.0004^{16}$ $1.2396 \pm 0.0013^{37}$
$\eta$	$0.05^6$	$0.0364 \pm 0.0004^{16}$ $0.0335 \pm 0.0025^{37}$
Random Exchange	$Fe_xZn_{1-x}F_2$ ( $H = 0$ )	Monte Carlo
$\alpha$	$-0.10 \pm 0.02^{17}$	$-0.051 \pm 0.013^{18}$
$\beta$	$0.350 \pm 0.009^{38}$	$0.3546 \pm 0.0028^{18}$
$\nu$	$0.69 \pm 0.01^{24}$	$0.6837 \pm 0.0053^{18}$
$\gamma$	$1.31 \pm 0.03^{24}$	$1.342 \pm 0.010^{18}$
$\eta$	$0.10^{24}$	$0.0374 \pm 0.0045^{18}$
Random Field	$Fe_xZn_{1-x}F_2$ ( $H > 0$ )	Monte Carlo & Exact Ground State
$\alpha$	$0.0 \pm 0.02^{17}$	$-0.5 \pm 0.2^{26}$ $-0.55 \pm 0.2^{39}$
$\beta$	not measured <sup>40</sup>	$0.00 \pm 0.05^{26}$ $0.02 \pm 0.01^{39}$
$\nu$	$0.88 \pm 0.05$	$1.1 \pm 0.2^{26}$ $1.14 \pm 0.10^{39}$
$\gamma$	$1.58 \pm 0.13$	$1.7 \pm 0.2^{26}$ $1.5 \pm 0.2^{39}$
$\eta$	$0.20 \pm 0.05$	$0.50 \pm 0.05^{26}$
$\bar{\gamma}$	$2\gamma = 3.16 \pm 0.26$	$3.3 \pm 0.6^{26}$ $3.4 \pm 0.4^{39}$
$\bar{\eta}$	$2\eta = 0.40 \pm 0.10$	$1.03 \pm 0.05^{26}$

TABLE IV. The  $d = 3$  Ising critical exponents obtained from experiments on the  $Fe_xZn_{1-x}F_2$  and the corresponding values from Monte Carlo simulations and exact ground state calculations. More extensive experimental, theoretical and simulation results are compared for the pure model in ref.<sup>37</sup> and<sup>16</sup> and for the random-exchange model in ref.<sup>18</sup> and<sup>41</sup>. Note that, unlike the pure and REIM cases, it is well established that hyperscaling is violated in the RFIM case<sup>11</sup>, i.e.  $\alpha + d\nu \neq 2$  for the RFIM.